Article

Rapid Screening of Effective Dopants for FeO Photocatalysts with Scanning Electrochemical Microscopy and Investigation of Their Photoelectrochemical Properties

Jum Suk Jang, Joowook Lee, Heechang Ye, Fu-Ren F. Fan, and Allen J. Bard

More About This Article

Additional resources and features associated with this article are available within the HTML version:

- Supporting Information
- Access to high resolution figures
- Links to articles and content related to this article
- Copyright permission to reproduce figures and/or text from this article

View the Full Text HTML

Rapid Screening of Effective Dopants for Fe₂O₃ Photocatalysts with Scanning Electrochemical Microscopy and Investigation of Their Photoelectrochemical Properties

Jum Suk Jang, Joowook Lee, Heechang Ye, Fu-Ren F. Fan, and Allen J. Bard*

Center for Electrochemistry, Department of Chemistry and Biochemistry, The University of Texas at Austin, Austin, Texas 78712

Scanning electrochemical microscopy in the photoelectrochemical (PEC) mode was used to search for more efficient doped iron oxide photocatalysts under visible light irradiation ($\lambda \geq 420$ nm). Iron oxide doped with one or two different metal cations was investigated to improve its PEC performance. Among various dopants, Sn or Ti as single dopants and Be or Al as codopants showed an improved photocurrent response of Fe₂O₃ under visible light irradiation ($\lambda \geq 420$ nm). Fe₂O₃ doped with 4% Sn(IV) and 6% Be(II) showed the highest photocurrent as well as a good photosensitivity and stability in alkali solution (0.2 M NaOH) under UV and visible light irradiation.

Introduction

Visible light-driven photocatalysts that can produce hydrogen from water splitting under solar light irradiation have been actively sought.[1-3] A photoelectrochemical (PEC) system is a potentially effective method of producing hydrogen from sunlight and water. While a great deal of progress has been made in our understanding of PEC systems, practical, inexpensive, efficient, and stable devices have not yet been realized. The search for efficient photocatalysts for water splitting under visible light irradiation has been approached from several directions: (i) to find new single phase materials,[4,5] (ii) to tailor the band gap by modifying cations or anions of UV or visible photocatalysts with substitutional doping,[6-8] (iii) to fabricate multicomponent photocatalysts by forming composites,[9-11] (iv) to decorate UV-active photocatalysts with a photosensitizer absorbing visible light,[12,13] and (v) to improve PEC properties of photocatalysts by loading or doping with a metal or noble metal.[14-16] Among various candidate materials, iron oxide very early on was considered a good candidate for a PEC system because of its small band gap (approximately 2.2 eV), good stability, convenient processing, and low cost.[17] The theoretical maximum efficiency of Fe₂O₃ is 12.9%.[18] Although iron oxide possesses many advantages, it has severe limitations, such as a small optical absorption coefficient in the visible region, short carrier diffusion lengths, and rapid electron−hole recombination rates.[19,20] Many studies have sought to improve the PEC properties of iron oxide by doping with various metals.[21-27] Most dopants have been shown to increase carrier concentrations, but some have decreased the photocurrent by introducing electron or hole traps. Sartoretti et al. reported that Fe₂O₃ doped with metal cations such as Al³⁺/Ti⁴⁺ and Zn²⁺/Ti⁴⁺ affected the hole diffusion length, leading to a negative shift of the photocurrent onset potential.[23] As a result of this doping, the photocurrent of a doped Fe₂O₃ thin film could be improved. Hu et al. prepared Pt-doped Fe₂O₃ thin films by an electrochemical route and reported improvement of the photocurrent compared to pure Fe₂O₃. Most research with doped Fe₂O₃ has focused on single dopants to improve its photoresponse.[26] By use of scanning electrochemical microscopy (SECM) in the PEC mode, arrays of doped materials may be rapidly screened; this can be used to quickly search and develop new photocatalysts sensitive to UV or visible light irradiation.

Recently our group reported a SECM method, modified by replacing the usual ultramicroelectrode (UME) tip with an optical fiber for rapid screening of photocatalysts,[28] analogous to the use of SECM for electrocatalyst discovery.[29] The optical fiber connected to a light source illuminates ∼300 µm diameter photocatalyst spots in an array, one at a time, and signals the photoactivity of each from the substrate current that is recorded at that spot. In the present work, we report the effects of various single and double dopants on the PEC effect of iron oxide using the SECM and measure the photocurrent of undoped and doped iron oxides in alkaline solution under UV and visible ($\lambda \geq 420$ nm) light irradiation.

Experimental Section

Preparation of Photocatalyst Spot Arrays. F-doped tin oxide (FTO) coated glass was obtained from Pilkington (Toledo, OH). Squares (15 mm × 15 mm) were cleaned by sonicating successively in ethanol and isopropanol and rinsed with deionized water. Fe(NO₃)₃·9H₂O (Aldrich) and ethylene glycol (Fisher) were used as received. All metal precursor solutions were made with ethylene glycol (EG) with a metal nitrate or chloride salt of concentration 0.2 and 0.04 M.

A CH Instruments model 1550 Dispenser (Austin, TX) was used to fabricate the photocatalyst arrays. The model 1550 consists of a stepper motor operating an XYZ stage with a piezodispenser (MicroJet AB-01-60, MicroFab, Plano, TX) attached to the head. The system is connected and controlled with a personal computer. The substrate (FTO) was placed under the piezodispenser tip. The XYZ stage moved the dispenser head in a preprogrammed pattern, while voltage pulses were applied to the piezodispenser to eject different numbers of ∼100 pL drops of the metal precursor solutions onto the substrate. The first component (metal precursor solution) was loaded and dispensed in a preprogrammed pattern onto the FTO substrate. After the piezodispenser was washed and flushed, the second metal precursor solution was loaded into the dispenser and dispensed into an overlaying pattern. These steps were repeated

6720 *J. Phys. Chem. C, Vol. 113, No. 16, 2009*

Jang et al.
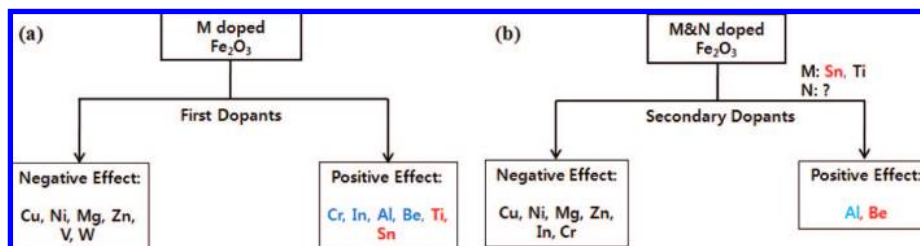
Figure 1. Summary of doping effects on Fe_2O_3 for a number of metals as found with the SPECM array.

when a third component was added. The patterned arrays were calcined at 500 °C for 3 h.

Screening the Spot Array. A schematic of the SECM setup in the PEC mode (abbreviated as SPECM) was depicted in a previous communication.[28] An optical fiber (FT-400-URT, 3M, St. Paul, MN) connected to a 150 W xenon lamp was attached to the tip holder of a CHI model 900B SECM. The array was placed in a SECM cell made of Teflon with the FTO/ photocatalyst working electrode exposed at the bottom through an O-ring. A Pt wire counter electrode and an Ag/AgCl reference electrode were used to complete the three-electrode configuration. The electrolyte was 0.2 M NaOH. Light from the xenon lamp was passed through the optical fiber, which was positioned perpendicular to the working electrode surface, and illuminated the working electrode. A 420 nm long-pass filter was used for visible light illumination experiments. The optical fiber tip was held and scanned 50 μm above the working electrode surface, while a potential bias was applied to the working electrode array via the FTO substrate. The photocurrent produced during the scan was measured and displayed as a two-dimensional image. Generally the applied potential was 0.2 V vs Ag/AgCl or about 0.4 V vs NHE, where the photoreaction is oxidation of hydroxide ion to oxygen, as demonstrated in earlier work.[28]

Preparation and Measurement of Photoelectrochemical Properties of Bulk Spot Array Electrode. A mixed solution containing metal precursor with specific compositions was prepared in ethylene glycol. Bulk spot array was fabricated on FTO-coated glass with a CH Instruments model 1550 Dispenser. The patterned bulk spot arrays were calcined at 500 °C for 3 h. The electrochemical cell was comprised of a thin film electrode (0.18 cm^2), Ag/AgCl, and Pt gauze as photoanode, reference electrode, and counter electrode, respectively. The photoanode was illuminated with a Xe lamp (150 W) equipped with a UV cutoff filter ($\lambda \geq 420$ nm). The photocurrent vs potential ($i-V$) was measured in a 0.2 M NaOH solution (pH = 13.3) under UV or visible light irradiation ($\lambda \geq 420$ nm). Chronoamperometry curves were obtained at 0.4 V vs Ag/AgCl for photosensitivity measurements of the electrode under dark or illuminated conditions.

Physicochemical Characterization. X-ray diffraction (XRD) measurements were carried out using a Bruker-Norius D8 advanced diffractometer. The CuK radiation source was operated at 40 kV and 40 mA. All measurements were carried out in the ($\theta/2\theta$) mode. Samples for XRD analysis were prepared using the same metal salt solution used to fabricate the photocatalyst arrays. The solutions were mixed in 25 mL vials according to the ratio determined by SPECM experiments and were then heated at 500 °C for 3 h. The optical properties of undoped and doped iron oxide films were analyzed with a UV–visible diffuse reflectance spectrophotometer (Milton Roy Spectronic 3000 Array).
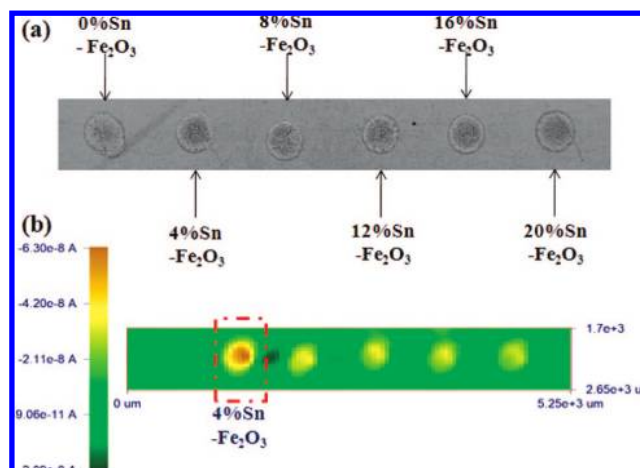
Figure 2. (a) Dispensed pattern of photocatalyst spot array with different mol % of Sn in Fe_2O_3. (b) SECM image measured with spot arrays at applied potential of 0.2 V vs Ag/AgCl in 0.2 M NaOH under visible light irradiation ($\lambda \geq 420$ nm).

Results and Discussion

Screening Arrays by SECM. To develop a doped iron oxide (Fe_2O_3) photocatalyst active for water or hydroxide oxidation under visible light illumination, we screened various candidates as single or double dopants. Different dopants exhibited positive or negative effects on the UV and visible light induced photocurrent response compared to undoped Fe_2O_3 as summarized in Figure 1. Spot arrays of Fe_2O_3 with different concentrations of various dopants (0–10% dopants in 2% or 4% increments) were fabricated and screened. For the screening of single dopants, the array pattern was prepared from solutions containing 0.2 M $Fe(NO_3)_3$ and 0.04 M dopant solutions as the nitrate salts as shown in Figure 2a. The first and sixth spots in the row were 100% Fe_2O_3 (20 drops of $Fe(NO_3)_3$) and 20% metal-doped Fe_2O_3, respectively. Figure 2b shows a typical SECM image obtained from a photocatalyst spot array consisting of Fe and Sn under visible light ($\lambda \geq 420$ nm). The sample spot with highest photocurrent had a dark brown color, while that with the smallest was dark green. Note that there is a small cathodic current of unknown origin on the FTO substrate at a potential of 0.2 V. Figure 3 shows the averaged photocurrent results obtained from multiple SPECM measurements. The largest photocurrent value was obtained at the 4% Sn–Fe spot (the values represent the atom percent relative to elemental iron), which was 8 times that of pure Fe_2O_3 (8 nA), and then decreased gradually with further increase in the amount of Sn. This may be caused by the change of cation charge of Fe^{3+} to Fe^{2+} and its amount in the photoactive material (Fe_2O_3). The addition of titanium to iron oxide also showed similar trends as that of tin dopant on Fe_2O_3 in the photocurrent (not shown). The mechanisms for the photocurrent enhancement by Sn^{4+}, Ti^{4+}, and

Screening of Dopants for Fe$_2$O$_3$ Photocatalysts

J. Phys. Chem. C, Vol. 113, No. 16, 2009 **6721**
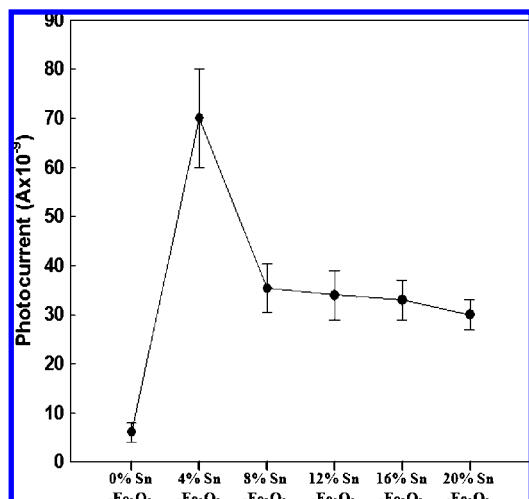
Figure 3. Photocurrents obtained from SECM spot array in Figure 2b. Electrolyte solution, 0.2 M NaOH; light source, 150 W Xe lamp; applied potential, 0.2 V vs Ag/AgCl.
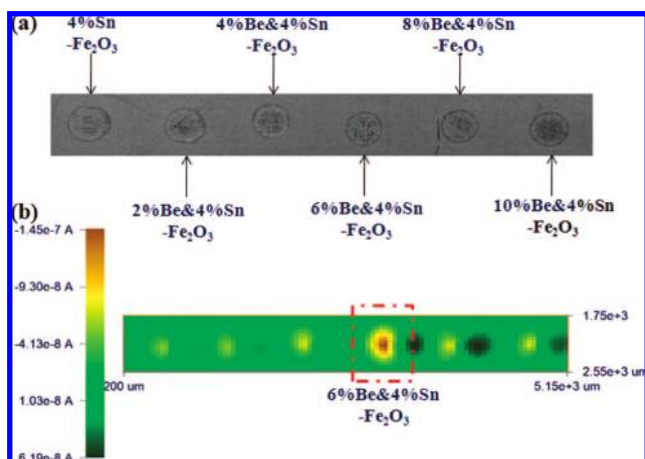
Figure 4. (a) Dispensed pattern of photocatalyst spot array with different mol % of Be in 4% Sn−Fe$_2$O$_3$. (b) SECM image measured with spot arrays at applied potential of 0.2 V vs Ag/AgCl in 0.2 M NaOH under visible light irradiation ($\lambda \geq$ 420 nm).

Si^{4+} as dopants on iron oxide have been proposed.[21−25] Fe in the hematite lattice is substituted by Sn or Ti. In the presence of ethylene glycol (a reducing agent), Sn(IV) and Ti(IV) might be reduced to lower oxidation states (i.e., Sn(II), Ti(III)) at high temperatures, and these could play the roles of electron donors, improving the electrical conductivity of hematite. In our work we also tested two dopants which produce a dramatic improvement in the photocurrent of Fe$_2$O$_3$ under visible light.

To investigate an effect of a second dopant on Fe$_2$O$_3$, we fixed 4% Sn as the first dopant. The array pattern was prepared from the mixture solution containing Fe and 4% Sn and another second dopant (0.04 M) as shown in Figure 4a. The first and sixth spots in a row are 4% Sn−Fe$_2$O$_3$ and 4% Sn−Fe$_2$O$_3$ with 10% of a second dopant, respectively. Among various second dopants, only Be^{2+} and Al^{3+} showed positive effects while all other dopants tested, such as Cu, Ni, Mg, Zn, In, and Cr, showed negative effects on the photocurrent response of 4% Sn−Fe$_2$O$_3$.

Figure 4b shows the SECM image obtained from photocatalyst spot arrays consisting of Fe, Sn, and Be under visible light ($\lambda \geq$ 420 nm) illumination. The largest photocurrent (130 nA) was observed at the composition of the 6% Be−4% Sn−Fe spot,
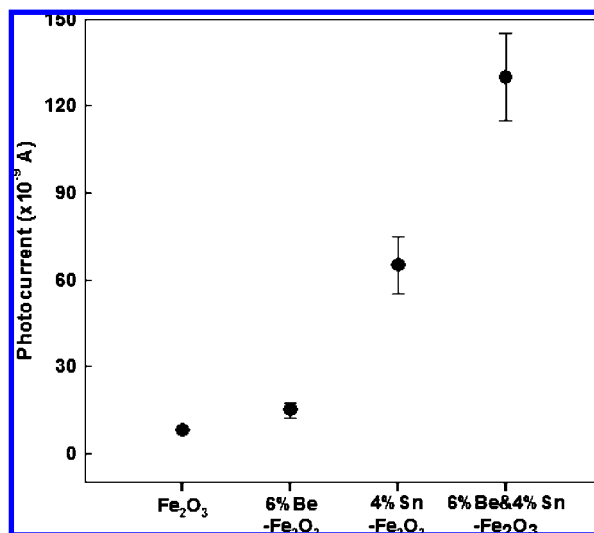
Figure 5. Photocurrents obtained from SECM spot array in Figure 4b. Electrolyte solution, 0.2 M NaOH; light source, 150 W Xe lamp; applied potential, 0.2 V vs Ag/AgCl.

which was twice that of the 4% Sn−Fe$_2$O$_3$ spot (65 nA). The photocurrent then decreased gradually with further increase of the amount of Be. It is not clear why second dopants such as Be and Al improve the photocurrent of Fe$_2$O$_3$ photocatalyst doped with Sn, although perhaps Be^{2+} can change the surface of Fe$_2$O$_3$ and Sn-doped Fe$_2$O$_3$ or control the amount of effective cation charge of Fe^{3+} to Fe^{2+} on the surface of photoactive material (Fe$_2$O$_3$).

Figure 5 shows the photocurrent calculated from SECM images of a Be−Sn−Fe$_2$O$_3$ spot array. The photocurrent generated under visible light irradiation ($\lambda \geq$ 420 nm) increased in the following sequence: 6% Be−4% Sn−Fe$_2$O$_3$ (130 ± 15 nA) > 4% Sn−Fe$_2$O$_3$ (65 ± 10 nA) > 6% Be−Fe$_2$O$_3$ (15 ± 2.5 nA) > Fe$_2$O$_3$ (8 ± 2 nA).

Al as the second dopant on Ti-doped Fe$_2$O$_3$ was first introduced by Sartoretti et al., who obtained the largest photocurrent from a 5% Ti^{4+} and 1% Al^{3+} doped iron oxide photoanode.[23] However, no study has been previously reported for Be as a second dopant for Sn-doped Fe$_2$O$_3$ photocatalyst. For further investigation on the bulk PEC properties of iron oxide with a second dopant, we kept the Be ratio to 6% on 4% Sn−Fe$_2$O$_3$.

Characterization. After screening studies, it is important to characterize the spot materials, at least in a preliminary way. Figure 6 shows the XRD patterns of the undoped and 4% Sn, 6% Be, and 4% Sn doped Fe$_2$O$_3$ photocatalyst. The phase of undoped or doped iron oxides formed via pyrolysis of iron(III) nitrate solution and the mixed solution containing dopants is primarily α-Fe$_2$O$_3$ (hematite). Sn- and Be-doped Fe$_2$O$_3$ did not show other impurity phases at the dopant levels used.

The optical properties of the undoped and doped thin films were measured by UV−visible absorption spectra and are displayed in Figure 7. Absorption of samples was observed around 590 nm (2.1 eV), a shoulder around 540 nm (2.3 eV), and a peak around 400 nm (3.1 eV). Note that the first two absorptions are much stronger, reflecting the selection rules. When the curves are normalized to the maximum absorbance of Fe$_2$O$_3$, one does not see any dramatic spectral change, with an "effective" band gap estimated from the absorption spectra of about 1.69 eV. This suggests that the observed effects cannot be attributed to improved absorption of incident radiation, but rather arise from kinetic effects on the photogenerated carriers.
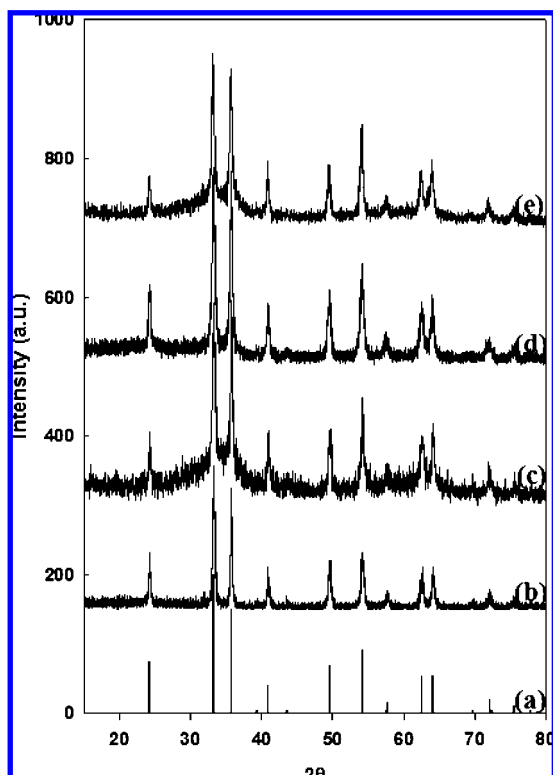
Figure 6. XRD patterns of (a) α-Fe$_2$O$_3$ (JCDPS 89-0599), (b) Fe$_2$O$_3$, (c) 6% Be−Fe$_2$O$_3$, (d) 4% Sn−Fe$_2$O$_3$, and (e) 6% Be and 4% Sn−Fe$_2$O$_3$ samples.
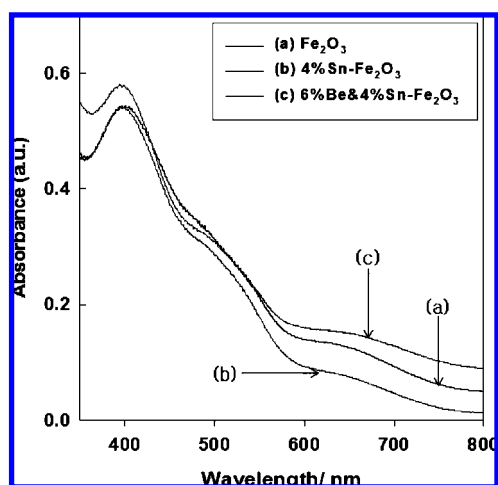
Figure 7. UV−visible spectra of (a) Fe$_2$O$_3$, (b) 4% Sn−Fe$_2$O$_3$, and (c) 6% Be and 4% Sn−Fe$_2$O$_3$ thin films.

Bulk Film Measurements. Once one finds apparently optimized materials in an array, it is useful to confirm the SECM results with those of bulk films of the same composition prepared in different ways on a larger electrode. As a first test we prepared a patterned bulk spot array of either undoped or doped Fe$_2$O$_3$ photocatalysts on FTO glass as shown in Figure 8. The PEC measurements were performed in a glass cell to facilitate the transmittance of light to the photoelectrode surface, and all spots were illuminated simultaneously with the xenon lamp (150 mW/cm^2). The working electrode had an active surface area of 0.18 cm^2, while a platinum gauze and an Ag/AgCl electrode were used as counter and reference electrodes, respectively. The electrolyte solution used for all measurements
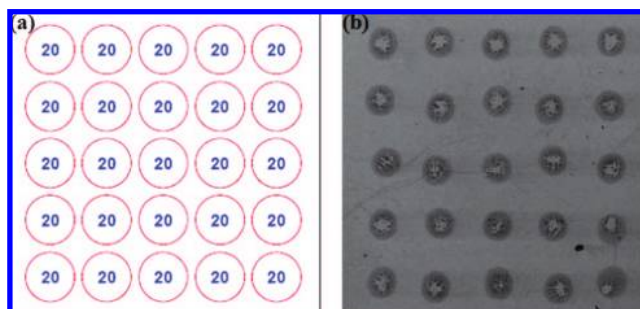
Figure 8. (a) Dispensed pattern of bulk spot array electrode. (b) SEM image of as-prepared pattern. Total number of drops is 20 in bulk spot array electrode. The spot size of the photocatalyst is ∼300 μm in diameter.
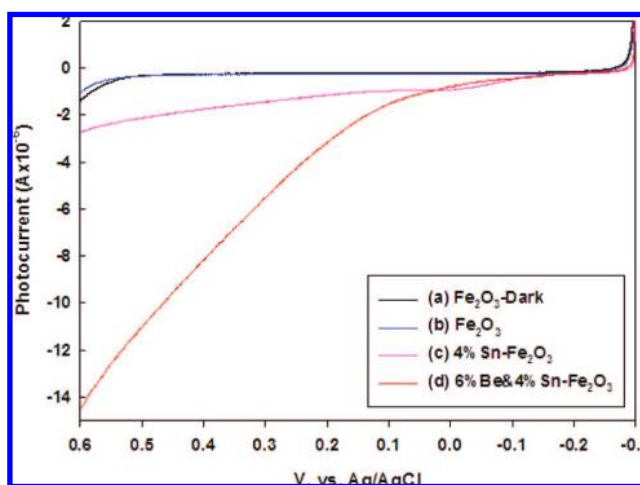
Figure 9. Photocurrent−potential curves of (a) Fe$_2$O$_3$ (dark), (b) Fe$_2$O$_3$, (c) 4% Sn−Fe$_2$O$_3$, and (d) 6% Be−4% Sn−Fe$_2$O$_3$ bulk spot array electrodes under visible light irradiation ($\lambda \geq 420$ nm). Electrolyte solution, 0.2 M NaOH; light source, 150 W Xe lamp. The sweep rate was 0.5 mV/s.

was 0.2 M NaOH. The doped iron oxide bulk spot array electrode showed higher photocurrents than that of the undoped pure Fe$_2$O$_3$ over a potential range of (−0.15)−(0.60) V, as shown in Figure 9. The Sn- or Sn−Be-doped Fe$_2$O$_3$ spot array electrode showed an onset photopotential of ∼−0.15 V vs Ag/AgCl, which is ∼0.35 V negative of the thermodynamic potential for water oxidation at pH 13.3. The undoped Fe$_2$O$_3$ spot array electrode showed a negligible photocurrent under visible light irradiation ($\lambda \geq 420$ nm), while the 6% Be−4% Sn−Fe$_2$O$_3$ spot array electrode exhibited the highest photocurrent of ca. 33 μA/cm^2 at 0.2 V vs Ag/AgCl in 0.2 M NaOH solution under visible light ($\lambda \geq 420$ nm).

Figure 10 shows the current−time transient responses of Fe$_2$O$_3$, 4% Sn−Fe$_2$O$_3$, and 6% Be−4% Sn−Fe$_2$O$_3$ multispot electrodes under chopped visible ($\lambda \geq 420$ nm) and UV illumination conditions. Both 4% Sn and 6% Be−4% Sn doped Fe$_2$O$_3$ spot arrays showed good photosensitivity and stability under UV and visible light, i.e., a higher photocurrent under illumination relative to the dark current and photostability in alkali solution. The undoped Fe$_2$O$_3$ showed a low photocurrent under UV light and negligibly small photocurrent under visible light ($\lambda \geq 420$ nm) as compared to doped Fe$_2$O$_3$ photocatalysts.

The flat-band potentials of the Fe$_2$O$_3$, 4% Sn−Fe$_2$O$_3$, and 6% Be−4% Sn−Fe$_2$O$_3$ spot array electrodes were estimated from the Mott−Schottky (M−S) plots ($1/C_{sc}^2$ vs E, where C_{sc} is the
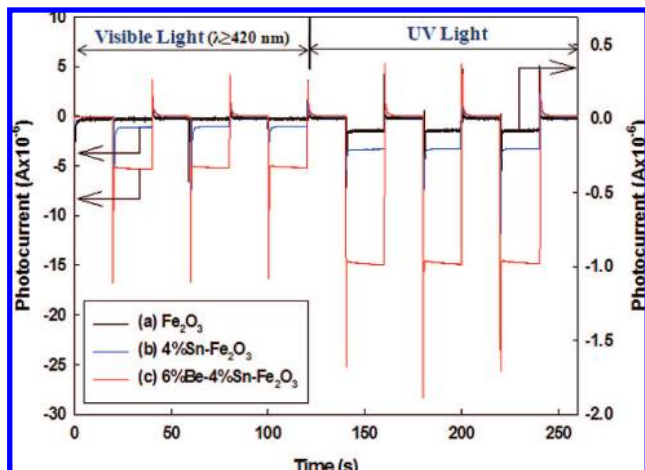
Figure 10. Chopped current−time transient response of (a) Fe₂O₃, (b) 4% Sn−Fe₂O₃, and (c) 6% Be−4% Sn−Fe₂O₃ bulk spot array electrodes under visible (λ ≥ 420 nm) and UV light irradiation. Electrolyte solution, 0.2 M NaOH; light source, 150 W Xe lamp; applied potential, 0.3 V vs Ag/AgCl.
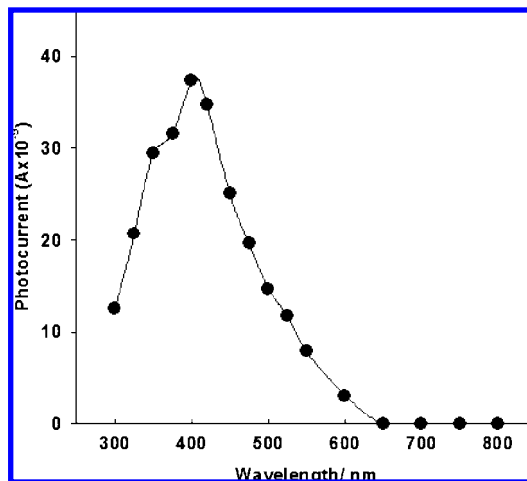
Figure 12. Photocurrent action spectrum of 6% Be−4% Sn−Fe₂O₃ bulk spot array electrode. Electrolyte solution, 0.2 M NaOH; light source, 150 W Xe lamp; applied potential, 0.3 V vs Ag/AgCl.
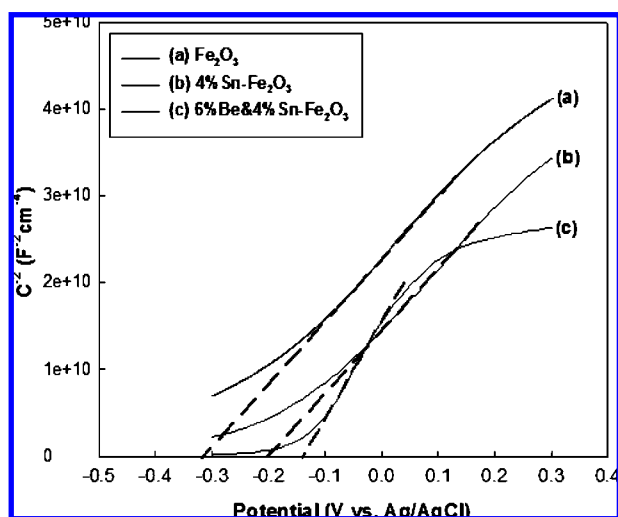
Figure 11. Mott−Schottky plots of (a) Fe₂O₃, (b) 4% Sn−Fe₂O₃, and (c) 6% Be−4% Sn−Fe₂O₃ bulk spot array electrodes in 0.2 M NaOH solution at 100 Hz under dark conditions.

space charge capacitance of the material). Figure 11 shows the M−S plots for the undoped and doped Fe₂O₃ spot array electrodes at pH 13.3 (0.2 M NaOH). Before and after doping with Sn or Sn and Be, the value of E_{fb} shifted positively from *ca.* −0.32 to −0.2 and −0.12 V, respectively, at pH 13.3. However, as generally found from such plots, there is often considerable uncertainty in the flat-band potentials estimated in this way,

Figure 12 shows the photocurrent action spectrum of a 6% Be and 4% Sn doped iron oxide spot array at a bias potential of 0.3 V vs Ag/AgCl. Under monochromatic illumination, the maximum photoresponse was observed at around 400 nm and the threshold wavelength on 6% Be−4% Sn−Fe₂O₃ spot is approximately 620 nm for the photoresponse, which nearly agrees with the absorption spectra[20,21] as shown in Figure 7. Note that the maximum power of the light source measured with a monochromator and power meter was about 475 nm. Thus, the photocurrent is mainly from direct transitions from the valence band orbitals to the conduction band edge (2p O²⁻

→ 3d Fe³⁺, 257−413 nm) and not from indirect transitions (d → d type, 564 nm).[30]

To evaluate the incident photon to current conversion efficiency (IPCE) of each undoped and doped Fe₂O₃ multispot array and from SECM image data, we used monochromatic irradiation with the optical fiber connected to the 150 W Xe lamp, coupled with a 420 nm band-pass filter (bandwidth ∼ 10 nm) where the incident radiation was calibrated with a power meter. The photocurrents generated by each spot in undoped and doped Fe₂O₃ arrays were measured using SECM. Figure 13 shows the monochromatic IPCE at 420 nm. The IPCE was calculated from the SPECM image, neglecting the geometric distribution of light in and outside of the spot and using the maximum photocurrent value. The IPCE of Fe₂O₃, 4% Sn−Fe₂O₃, and 6% Be−4% Sn−Fe₂O₃ spot array was about 0.14, 0.7, and 1.2%, respectively, at 0.3 vs Ag/AgCl, and displayed a similar trend as the increase of photocurrent shown in Figure 5. The inset figure shows the SPECM image of the 6% Be−4% Sn−Fe₂O₃ spot. Although the IPCE of Fe₂O₃ increased by doping with Sn and Be, the value is still rather small. However, it might be possible to improve the photocurrent further by optimizing the fabrication method for Fe₂O₃ thin film electrodes.[21−23]

Effect of Dopants. Although theoretical modeling of semiconductor materials has not yet allowed prediction of the effects of metal doping, the SPECM screening results, as summarized in Figure 1, show that the addition of many metals caused a decrease (negative effect) in the PEC performance, while relatively few caused a significant increase (positive effect). Dopants such as Sn, Ti, Cr, In, Al, and Be showed a positive effect while Cu, Ni, Mg, Zn, V, and W showed a negative effect on the photocurrent vs undoped Fe₂O₃. Among the dopants with a positive effect, Sn and Ti showed the greatest improvement in photocurrent of an iron oxide thin film. This rapid screening (combinatorial) approach may eventually provide guidelines to suggest effective candidates for photosplitting of water. A number of different processes come into play in determining the PEC efficiency, including the absorbance of the semiconductor, the efficiency of electron−hole pair separation, the thickness of the space charge layer, and electron−hole recombination that can be promoted by trap states in the bulk and on the surface.
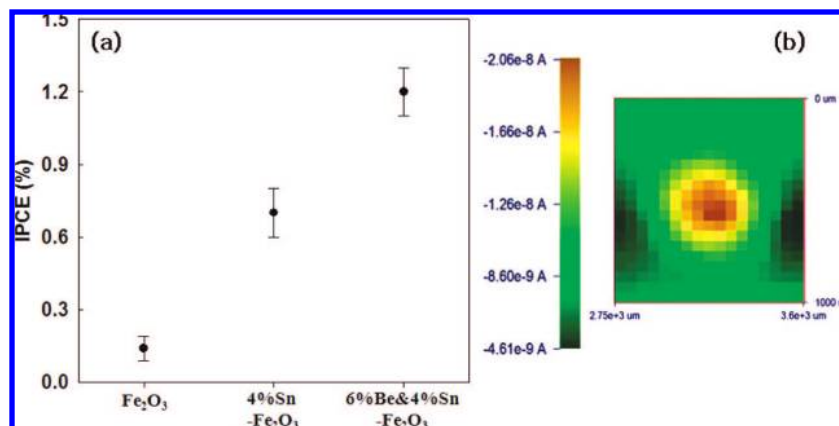
Figure 13. (a) IPCE of Fe_2O_3, 4% Sn−Fe_2O_3, and 6% Be−4% Sn−Fe_2O_3 spot array. Electrolyte solution, 0.2 M NaOH; light source, 150 W Xe lamp, band-pass filter, 420 nm; applied potential, 0.3 V vs Ag/AgCl. (b) SECM image of 6% Be−4% Sn−Fe_2O_3 spot. Incident photon flux at 420 nm is 9×10^9 (photons/s).

Conclusion

We successfully screened single and double dopants of Fe_2O_3 with SPECM to develop an improved doped Fe_2O_3 photocatalyst. Sn^{4+}, Ti^{4+} as single dopants, and Be^{2+}, Al^{3+} as second dopants of Fe_2O_3 showed the highest photocurrent under visible light irradiation ($\lambda \geq 420$ nm). Among various dopants and concentrations, 6% Be and 4% Sn doped Fe_2O_3 showed the highest photocurrent as well as stability in alkali solution (0.2 M NaOH) under UV and visible light irradiation. The IPCE of Fe_2O_3, 4% Sn−Fe_2O_3, and 6% Be−4% Sn−Fe_2O_3 spot arrays obtained at 420 nm and 0.3 V vs Ag/AgCl was 0.14, 0.7, and 1.2%, respectively.

References and Notes

(1) Fujishima, A.; Honda, K. *Nature (London)* **1972**, *238*, 37.
(2) Mau, A. W. H.; Huang, C. B.; Kakuta, N.; Bard, A. J.; Campion, A.; Fox, M. A.; White, J. M.; Webber, S. E. *J. Am. Chem. Soc.* **1984**, *196*, 6537.
(3) Park, J. H.; Kim, S.; Bard, A. J. *Nano Lett.* **2006**, *6*, 24.
(4) Kim, H. G.; Hwang, D. W.; Lee, J. S. *J. Am. Chem. Soc.* **2004**, *126*, 8912.
(5) Kudo, A.; Omori, K.; Kato, H. *J. Am. Chem. Soc.* **1999**, *121*, 11459.
(6) Maeda, K.; Teramura, K.; Takata, T.; Hara, M.; Saito, N.; Toda, K.; Inoue, Y.; Kobayashi, H.; Domen, K. *J. Phys. Chem. B* **2005**, *109*, 20504.
(7) Asahi, R.; Ohwaki, T.; Aoki, K.; Taga, Y. *Science* **2001**, *293*, 269.
(8) Zou, Z.; Ye, J.; Sayama, K.; Arakawa, H. *Nature (London)* **2002**, *424*, 625.
(9) Kim, H. G.; Borse, P. H.; Choi, W.; Lee, J. S. *Angew. Chem., Int. Ed.* **2005**, *44*, 4585.
(10) Wang, D.; Zou, Z.; Ye, J. *Chem. Mater.* **2005**, *17*, 3255.
(11) Kim, H. G.; Jeong, E. D.; Borse, P. H.; Jeon, S.; Yong, K. J.; Lee, J. S.; Li, W.; Oh, S. H. *Appl. Phys. Lett.* **2006**, *89*, 064103.
(12) Hagiwara, H.; Ono, N.; Inoue, T.; Matsumoto, H.; Ishihara, T. *Angew. Chem., Int. Ed.* **2006**, *45*, 1420.
(13) Park, J. H.; Bard, A. J. *Electrochem. Solid State Lett.* **2005**, *8*, G371.
(14) Arai, N.; Saito, N.; Nishiyama, H.; Domen, K.; Kobayashi, H.; Sato, K.; Inoue, Y. *Catal. Today* **2007**, *129*, 407.
(15) Maeda, K.; Teramura, K.; Lu, D.; Saito, N.; Inoue, Y.; Domen, K. *J. Phys. Chem. C* **2007**, *111*, 7554.
(16) Bae, S. W.; Borse, P. H.; Lee, J. S. *Appl. Phys. Lett.* **2008**, *92*, 10410.
(17) Hardee, K, L.; Bard, A. J. *J. Electrochem. Soc.* **1976**, *123*, 1024.
(18) Murphy, A. B.; Barnes, P. R. F.; Randeniya, L. K.; Plumb, I. C.; Grey, I. E.; Horne, M. D.; Glasscock, J. A. *Int. J. Hydrogen Energy* **2006**, *31*, 1999.
(19) Kennedy, J. H.; Frese, K. W. *J. Electrochem. Soc.* **1978**, *12*, 709.
(20) Dare-Edwards, M.; Goodenough, J. B.; Hamnett, A.; Trevellick, P. R. *J. Chem. Soc., Faraday Trans. 1* **1983**, *79*, 2027.
(21) Kay, A.; Cesar, I.; Grätzel, M. *J. Am. Chem. Soc.* **2006**, *128*, 15714.
(22) Duret, A.; Grätzel, M. *J. Phys. Chem. B* **2005**, *109*, 17184.
(23) Sartoretti, C. J.; Alexander, B. D.; Solarska, R.; Rutkowska, I. A.; Augustynski, J.; Cerny, R. *J. Phys. Chem. B* **2005**, *109*, 13685.
(24) Glasscock, J. A.; Barnes, P. R. F.; Plumb, I. C.; Savvides, N. *J. Phys. Chem. C* **2007**, *111*, 16477.
(25) Aroutiounian, V. M.; Arakelyan, V. M.; Shahnazaryan, G. E.; Hovhannisyan, H. R.; Wang, H.; Turner, J. A. *Sol. Energy* **2007**, *81*, 1369.
(26) Hu, Y. S.; Kleiman, S. A.; Forman, A. J.; Hazen, D.; Park, J. N.; McFarland, E. W. *Chem. Mater.* **2008**, *20*, 3803.
(27) Ingler, W. B.; Baltrus, J. P.; Khan, S. U. M. *J. Am. Chem. Soc.* **2004**, *126*, 10238.
(28) Lee, J.; Ye, H.; Pan, S.; Bard, A. J. *Anal. Chem.* **2008**, *80*, 7445.
(29) Fernandez, J. L.; Walsh, D. A.; Bard, A. J. *J. Am. Chem. Soc.* **2005**, *127*, 357.
(30) Cherepy, N. J.; Liston, D. B.; Lovejoy, J. A.; Deng, H.; Zhang, J. Z. *J. Phys. Chem B* **1998**, *102*, 770.